Polycarbonate nanocomposite with improved fire behavior, physical and psychophysical transparency

H. Vahabi, Olivier Eterradossi, L. Ferry, C. Longuet, R. Sonnier, José-Marie Lopez-Cuesta

Polycarbonate nanocomposite with improved fire behavior, physical and psychophysical transparency

H. Vahabi, O. Eterradossi, L. Ferry *, C. Longuet, R. Sonnier, J.-M. Lopez-Cuesta

Centre de Recherche CMGD, Ecole des Mines d'Alès, 6 avenue de Clavières, F-30319 Ales Cedex, France

A B S T R A C T

Transparent polycarbonate nanocomposites with improved fire behavior were prepared by incorporation of polyhedral oligomeric silsesquioxane (POSS) and resorcinol bis (diphenyl phosphate) (RDP) via melt blending. Flame retardancy performance was characterized using thermogravimetric analysis, pyrolysis combustion flow calorimeter and cone calorimeter. Simultaneous presence of RDP and POSS led to the decrease of the degradation rate and the increase of char residue due to the reaction of the additives with the decomposing polymer. This results in a significant reduction of flammability of polycarbonate. In cone calorimeter, the heat release rate as well as the smoke production rate were shown to strongly decrease due to a condensed phase mechanism that favored the formation of a cohesive char layer. Transparency evaluation was performed in both physical and psychophysical spaces. The two approaches give various assessment of transparency. Considering the perceived optical properties, it could be concluded that flame retarded PC is translucent rather than transparent.

Keywords:
Polycarbonate
Transparency
Flame retardancy
Polyhedral oligomeric silsesquioxane

1. Introduction

Polycarbonate (PC) is an important and widely used engineering thermoplastic. The annual volume of this polymer exceeds 1 million metric tons [1]. PC is an amorphous polymer with some outstanding mechanical properties [2]. Moreover, it is a high thermal stable polymer with the relatively high tendency to charring during combustion. Therefore, PC by itself shows a V-2 rating in the UL-94 test [3]. Furthermore, PC is a transparent polymer with exceptional clarity.

Over the past decade, optically transparent polymers have attracted considerable attention in numerous applications including protective face shields and eyewear, high-performance transportation glazing, high performance optical components, and electronic display screens [4–8]. In some sectors, i.e. construction materials or fire safety equipments, both good transparency and fire resistance properties are needed. Thus, PC seems to be an appropriate polymer for these applications. However, a further improved fire resistance property is often required. Among the different ways to improve the flame resistance of polymers, introduction of fillers has been widely investigated and was proved to be an efficient method [9–11]. Nevertheless, it has been reported that the introduction of fillers in PC can disrupt matrix transparency [12]. The major factor of loss of transparency is light scattering because of local refractive index variations. Some other parameters also influence the composite transparency, such as filler concentration, particle size, surface roughness and achieved dispersion state [12,13]. Achieving a high level of transparency with incorporation of nanoparticles is a challenge: since transparency is highly sensitive to the number of interfaces crossed by light, as well as to spatial organization (size, spatial density and orientation) of domains with different refractive indices [14]. Due to this interaction, transparency has to be expressed not only as a physical parameter depending mainly on angle-dependent transmittance, but also as perceived (or psychophysical)

* Corresponding author. Tel.: +33 4 66 78 53 58; fax: +33 4 66 78 53 65.
E-mail address: laurent.ferry@mines-ales.fr (L. Ferry).

transparency which accounts for the way transparent objects interact visually with their back- and foreground.

Among the different nanoparticles, incorporation of polyhedral oligomeric silsesquioxane (POSS) into polymers offers outstanding properties including optical transparency [15]. POSS molecules possess a cage-like structure (1–3 nm in size) and a hybrid chemical composition ($RSiO_{1.5}$) which is intermediate between silica (SiO_2) and silicones (R_2SiO) [16]. Some studies have shown the interest of POSS to improve flame retardancy of PC [17,18]. These studies showed that POSS is efficient for reducing the peak of heat release rate (pHRR). However, it is revealed that the combination of nanoparticles and conventional flame retardant (FR) (e.g. phosphorous compounds) is necessary to achieve a high level of flame resistance, with reduction of total heat release (THR) [19]. The use of phosphorous FR in PC has been investigated by different authors [3]. Among phosphorous FR, resorcinol bis (diphenyl phosphate) (RDP) has shown a good compatibility with PC and also has improved its fire resistance. RDP, which acts mainly in the condensed phase, tends to promote more char formation from PC, thus limiting fuel supply to the flame and effectively decreasing the temperature of the flame [3]. Furthermore, some works have shown synergistic effects of simultaneous presence of fillers and phosphorous flame retardants [20,21]. It was assumed that phosphorous compounds promote the formation of char layer while POSS enhances the thermo-oxidative resistance of this protective layer.

In this work, the influence of combinations of POSS and RDP on thermal stability, fire behavior and transparency of polycarbonate has been investigated.

2. Experimental part

2.1. Materials

Polycarbonate (PC) used was Makrolon® AL2647 from Bayer. Drying before processing was performed at 80 °C for 24 h under vacuum. Trisilanolphenyl-POSS (SO1458) was used as purchased from Hybrid Plastics, Inc. Resorcinol bis (diphenyl phosphate) (Fyrolflex® RDP) was supplied by ICL-IP company (Fig. 1).

2.2. Instrumentation

All blends were prepared using a micro-compounder (DSM) (twin screw: speed = 180 rpm, 4 min, T = 280 °C, capacity = 15 cm^3). The pellets were injection molded using a Krauss Maffei 50t apparatus (T = 200–240 °C, mold temperature = 80 °C). The thermal decomposition was investigated using a Perkin Elmer Pyris-1 TGA. All measurements were performed under nitrogen and air with a heating rate of 10 °C min^{-1}. The sample weight was 8 ± 2 mg. A Scanning Electron Microscopy (FEI Quanta 200 SEM) was used to study the morphology of the samples. All images were obtained under high vacuum at a voltage of 25.0 kV with a spot size of 3.0 nm. Evaluation of the flammability properties was made using Pyrolysis combustion flow calorimeter (PCFC) and cone calorimeter equipments produced by fire test technology (FTT). In PCFC tests, the samples (2 ± 0.5 mg) are heated at 1 K s^{-1} from 20 °C to 750 °C in a pyrolyzer and the degradation products are transported by an inert flux, and then mixed with oxygen before entering a combustor at 900 °C where the decomposition products are completely oxidized. The heat release rate (HRR) is measured as function of temperature according to oxygen depletion method (13.1 MJ of energy is released when 1 kg of oxygen is consummated according to Huggett's relation). Cone calorimeter tests were carried out on 100 × 100 × 4 mm^3 plaques using an incident heat flux of 35 kW m^{-2}, according to ISO 5660 standard. Total heat release (THR) and peak of heat release rate (pHRR) were obtained as main data, according to the same method as above. The X-ray diffraction (XRD) patterns were recorded using a Bruker AXS D8 Advance 104 diffractometer with CuKα radiation and a Vantec detector. The scanning range was from 2.5° to 45° with a step size of 0.007° and step time of 24.6 s. All measurements were taken using a generator voltage of 40 kV and a generator current of 40 mA.

Transparency evaluation was performed in both physical and psychophysical spaces. Physical transparency refers to instrumental values of transmitted intensities measured as a function of angle, while psychophysical transparency refers to the evaluation of parameters which elicit perceived transparency (mainly background contrast alteration and sharpness of reflected light source image). Physical transparency was evaluated in the visible range (380–780 nm). Photometric transmittance was recorded in the incidence plane under normal incidence using a goniospectrophotometer (GON-360 goniometer + MAS 40 Mini Array Spectrophotometer, Instrument Systems). The angular domain covered 20° on both sides of the specular transmission direction at 1° intervals. Psychophysical transparency was assessed using a contrast approach relying on Kitaoka's [22] work on object transparency. A 500 cm^2 BYK-Gardner unsealed paper penetration card

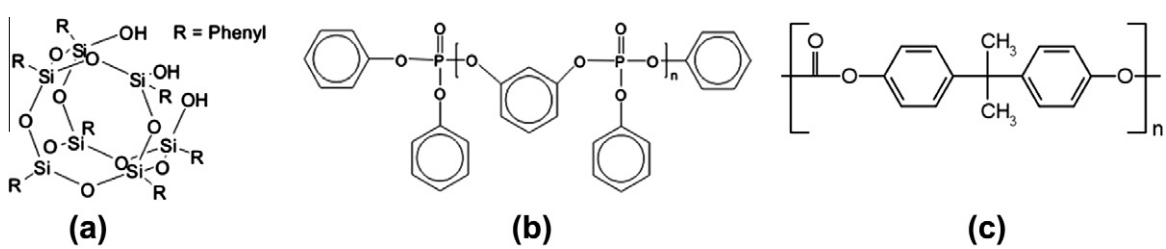

Fig. 1. Chemical structure of (a) POSS, (b) RDP and (c) PC.

(Model reference = 2805) was used as a background to avoid gloss artifacts. Both background and samples were placed in an upright position at a distance of 40 mm and lit from above by natural, diffuse ambient light. Photographs were taken using a CANON EOS 300 D camera in manual mode with EFS 18–55 lens used at 35 mm focal length, at an aperture of 22. Images were stored as RAW files. According to Kitaoka's formalism (Fig. 13), two parameters "α and t" are necessary to describe perceived transparency. "α" is a characteristic of background contrast alteration by an interposed object that does not fully cover the background (otherwise the problem shifts to perception of layer transparency). "t" stands for the front reflectance on the interposed object surface. Mean values of the four fields required to compute both α and t parameters were extracted from images using the *R* environment for statistical computing [23], and normalized to a [0.255] scale. Formulas for α and t are given in the header of Table 4. For obvious reasons, these formulas are autocalibrated, and account for illuminance variations which may arise from using natural ambient lighting.

3. Results and discussion

3.1. Microstructure

The SEM images of PC/POSS and PC/POSS/RDP blends are shown in Fig. 2. The image of PC/POSS sample shows POSS aggregates in the [500–700 nm] size range. Various research works have pointed out the formation of POSS aggregates in PC [2,24,25] and some interpretations have been proposed, such as the melt crystallization of POSS, the incompatibility between the POSS and PC matrix and the formation of intermolecular hydrogen bonds of hydroxyl groups of POSS molecules.

Furthermore, the size of POSS aggregates was decreased in the presence of RDP (in PC/POSS/RDP blend) and a more homogeneous dispersion was obtained, compared to PC/POSS sample. For PC/POSS and PC/POSS/RDP compositions, an interface between POSS aggregates and PC is observed, showing a lack of adhesion between aggregated particles and matrix. The decrease of aggregate size in PC/POSS/RDP sample can be explained by the presence of RDP which could be located on the surface of POSS particles thereby avoiding the aggregation. The chemical structure of RDP seems to confer surfactant properties to POSS molecules [26,27].

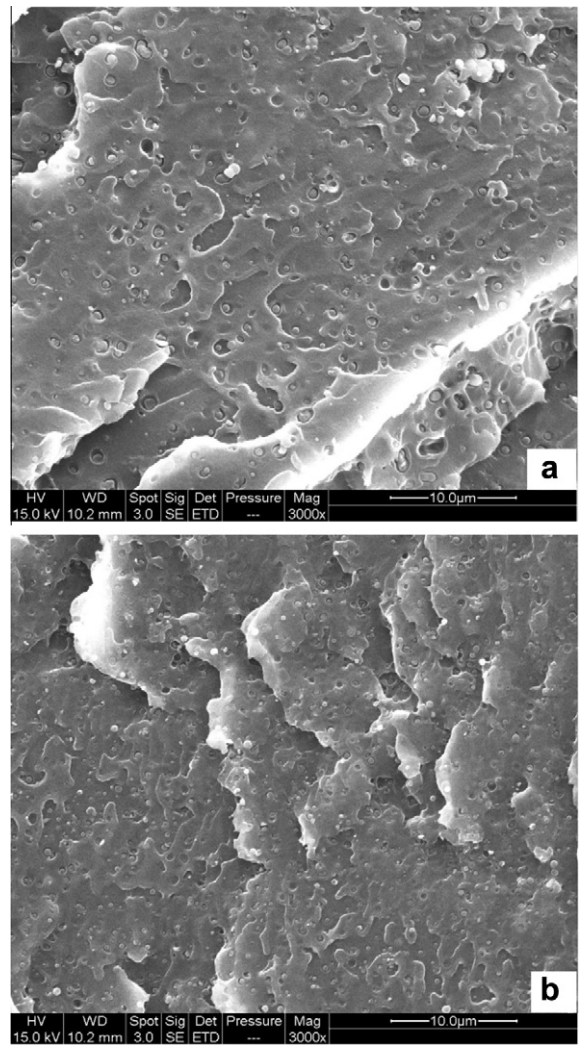

Fig. 2. SEM images of (a) PC/POSS and (b) PC/POSS/RDP samples.

3.2. Thermal and fire behavior

3.2.1. Thermogravimetric analysis (TGA)

The thermogravimetric (TGA) and differential thermal (DTG) analysis curves of all samples under nitrogen are shown in Fig. 3. The corresponding TGA parameters are given in Table 1. Tests made under nitrogen have shown that all materials degrade in a single step. The degradation of PC and PC/POSS respectively started at 425 and 450 °C while those of PC/RDP and PC/POSS/RDP samples started earlier around 335 °C. It was shown by Murashko et al. [28] that RDP starts to degrade at low temperature c.a. 320 °C. The volatilization products of RDP are likely to catalyze the Fries rearrangement reactions leading to an enhancement of PC charring. Moreover these volatilization products may also react with PC by transesterification inducing the accumulation of phosphorous in the char. Adding POSS in PC decreased the maximum degradation rate of PC by approximately 20%. The thermal degradation of POSS occurred in two steps (around 245 and 615 °C) (Supporting data). The first step is ascribed to the loss of water from the condensation reactions between two POSS molecules. This step of degradation corresponds to 3 wt.% of weight loss which can be in accordance with the loss of water molecules. The second step of degradation of POSS (at 540 °C) seems to have an important role since it appears to modify the thermal degradation pathway of PC. The thermal degradation of PC/POSS blend was investigated by Song et al. [29] and a mechanism of degradation has been proposed.

The authors [29] suggested that the volatile products from thermal degradation of PC (e.g. the alkyl substituted phenol) react with the free OH of POSS and increase the

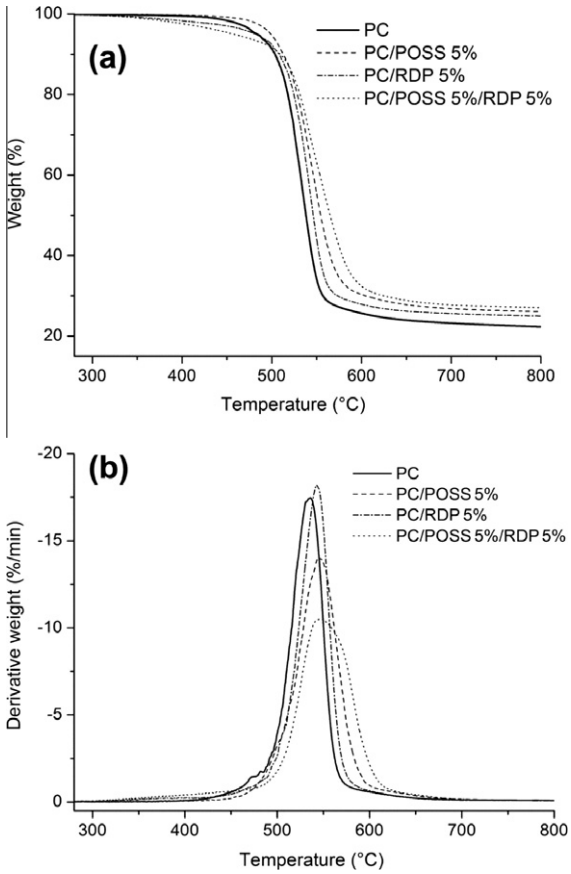

Fig. 3. Thermogravimetric analysis (a) and differential thermogravimetry curves (b) for PC, PC/POSS and PC/POSS/RDP at a heating rate of 10 °C/min under nitrogen.

Table 1
TGA parameters of PC, PC/POSS, PC/RDP and PC/POSS/RDP samples under nitrogen.

Composition	O_{nset} (°C)	$T_{5wt.\%}$ (°C)	$T_{50wt.\%}$ (°C)	Char (wt.%)*
PC	424	482	537	22
PC/POSS 5%	449	500	555	26
PC/RDP 5%	336	479	546	25
PC/POSS 5%/RDP 5%	336	453	565	27

* Char residue at 800 °C.

thermal stability of PC. Moreover, when the temperature increases, the phenyl groups of POSS are released and improve the thermal stability via a crosslinking process with the degradation products of PC. TGA curves of POSS and PC/POSS (Supporting data and Fig. 3, respectively) indicate that the improvement of thermal stability of PC (occurred after 550 °C) is simultaneous with the second step of degradation of POSS. This stage of degradation of POSS corresponds to the release of phenyl groups.

PC/POSS/RDP composition exhibited the highest char yield at 800 °C (27 wt.%) among all samples. Moreover the maximum degradation rate is strongly decreases and

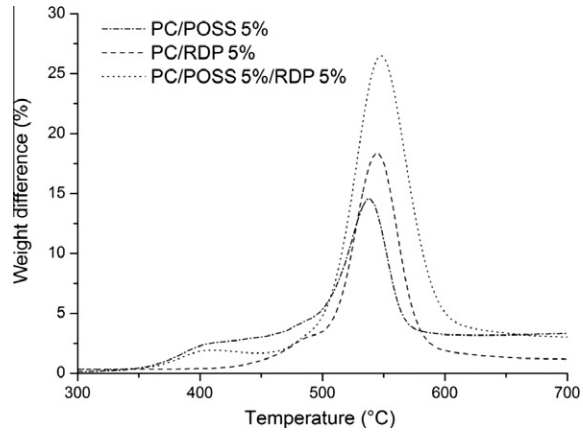

Fig. 4. Difference between experimental and calculated TG curves.

shifted to high temperature while the release of gases occurs within a wider range of temperature.

In order to investigate further interactions between FR additives and PC, expected TGA curves of binary or ternary systems have been calculated from the weight loss of components using the mixing rule. The difference between experimental and calculated curves is plotted on Fig. 4. The results indicate that RDP starts to interact with the polymer matrix from 350 °C, i.e. before the onset of PC degradation. This speaks in favor of the hypothesis of volatilization products transesterification. The highest interaction is evidenced around 540 °C, that is the maximum of PC degradation rate, indicating that RDP interferes also with the polymer chain scission mechanism. In the case of POSS, interactions start simultaneously with PC degradation, inducing a thermal stabilization equal or even higher than that of RDP. Finally the POSS/RDP system acts not only at low temperature similar to pure RDP but also during PC degradation. In this latter range, the combination of additives leads to the highest interactions with a weight loss 27% lower than expected. Moreover, the maximum of the difference between experimental and theoretical curve is shifted to high temperature. Both outcomes (shift and increase of weight mismatch) indicate a synergistic effect between POSS and RDP that may be due to a better dispersion of POSS in the presence of RDP as it was shown in the proceeding section.

In nitrogen atmosphere, the degradation rate exhibits the lowest values for PC/POSS/RDP samples (decrease of peak of DTG curve- Fig. 3).

3.2.2. Pyrolysis combustion flow calorimeter (PCFC) test

Flammability of samples was measured using microcalorimeter test. Fig. 5 displays the heat release rate curves of PC, PC/POSS, PC/RDP and PC/POSS/RDP samples. All samples present a single peak of HRR (pHRR) at a similar temperature (around 540 °C). The values of pHRR are respectively 419, 354 (−15.5%), 373 (−11.1%) and 341 (−18.5%) W/g for PC, PC/POSS, PC/RDP and PC/POSS/RDP. Thus the decrease of pHRR follows the same trend than that of the weight loss rate as determined by TGA.

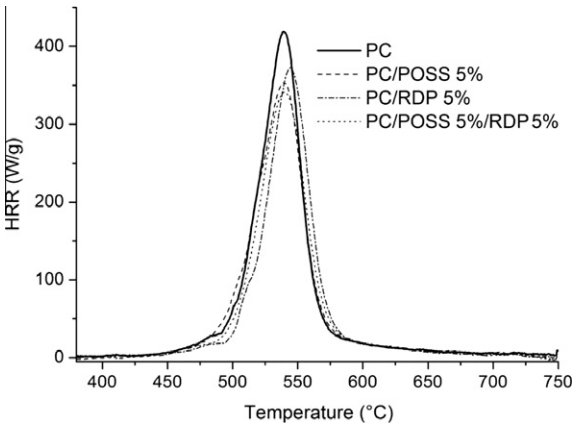

Fig. 5. Heat release rate curves of PC, PC/POSS and PC/POSS/RDP.

The THR of PC slightly decreases in the presence of POSS, RDP or POSS/RDP. However, there are not important differences between THR values for PC/POSS, PC/RDP and PC/POSS/RDP samples. It can be concluded that the flammability properties are mainly governed by the pyrolysis of the condensed phase and not by chemical effects in the vapor phase.

3.2.3. Cone calorimeter test

Cone calorimeter tests were performed under an irradiance of 35 kW m^{-2}. HRR curves versus time for PC, PC/POSS, PC/RDP and PC/POSS/RDP samples are represented in Fig. 6 and the main parameters of this test are reported in Table 2. Times to ignition of PC/POSS, PC/RDP and PC/POSS/RDP are reduced compared to pure PC. This reduction may be attributed to the release of volatile products by POSS and RDP at low temperature as it was evidenced by TGA. After ignition HRR increases before reaching a peak and stabilizing. This behavior is typical of the formation of a protective layer at the surface of the sample that controls the heat and mass transfer and thus the pyrolysis rate. The peak of HRR is reduced by adding the POSS and RDP to PC. However, these values do not show significant differences between PC/POSS, PC/RDP

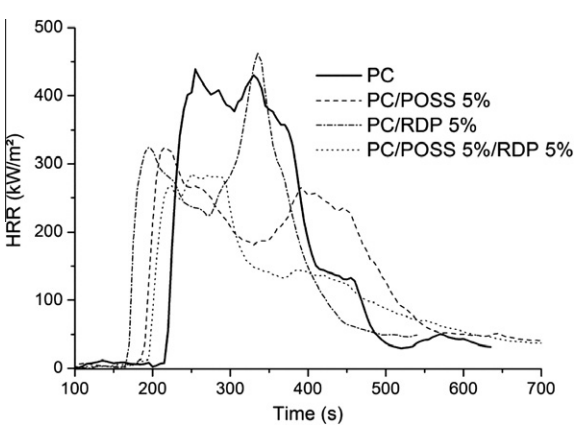

Fig. 6. HRR curves for PC, PC/POSS, PC/RDP and PC/POSS/RDP.

Table 2
Parameters of cone calorimeter test for PC, PC/POSS, PC/RDP and PC/POSS/RDP samples.

Composition	TTI (s)	pHRR-1* (kW m^{-2})	pHRR-2** (kW m^{-2})	THR (MJ m^{-2})
PC	214	439	431	82
PC/POSS 5%	184	322	266	86
PC/RDP 5%	164	322	461	75
PC/POSS 5%/RDP 5%	194	284	144	64

* First peak of HRR curve.
** Second peak of HRR curve.

and PC/POSS/RDP samples up to 300s. The major difference of pHRR is observed after 300s. THR values of PC/RDP and PC/POSS/RDP samples are decreased compared to pure PC.

All samples showed the typical thick charring behavior [30]. PC, PC/POSS and PC/RDP samples present a second additional distinct peak which may be caused by the cracking of the char formed [30] (at 330s for PC, 392s for PC/POSS and 335s for PC/RDP). For PC/POSS/RDP sample, the second shoulder (peak) is less distinct. Fig. 7 shows the image of residues after cone calorimeter tests. The quantity and size of formed char is more important in the case of PC/POSS/RDP samples and seems more expanded (Unfortunately, the measurement of mass loss versus time for some tests was disrupted due to contact of char with cone part of cone calorimeter device).

The formation of this important quantity of char can delay and decrease the cracking of the protecting layer. Therefore, the release of gases, which were captured under the protect layer, and the diffusion of oxygen into polymer bulk are also limited. Furthermore, this char acts as a thermal insulation for underlying polymer and reduces the heating of material and therefore the second HRR peak decreased. The comparison of total smoke release curves of these samples (Fig. 8) confirms the significant reduction of smoke release for PC/POSS/RDP sample after 300s due to the formation of important charred, cohesive and expanded structure, compared to other samples, which prevents soot emission.

3.2.4. X-ray diffraction (XRD) of residues

Fig. 9 displays the XRD patterns of initial POSS (a) and heated POSS (200 °C (b), 400 °C (c) and 700 °C (d)). The initial POSS has a crystalline structure and a distinct peak at $2\theta = 7°$ is typical of this kind of POSS [31]. This POSS was heated in air atmosphere at 3 isothermal temperatures and the residues were analyzed using XRD.

Spectra of heated POSS at 200 and 400 °C (b and c) show the loss of crystallinity. However, a broad peak at $2\theta = 7°$ remained. Finally, an amorphous structure was obtained at 700 °C.

These XRD spectra were compared to those of char residue from cone calorimeter test of respectively PC (e) and PC–POSS–RDP (f: top of the residue, g: bottom of the residue). It can be noted that the top of PC–POSS–RDP residue exhibits a XRD spectrum very close to that of PC whereas the structure of residue bottom looks like heated POSS. The formation of a complex amorphous silico-carbonaceous is

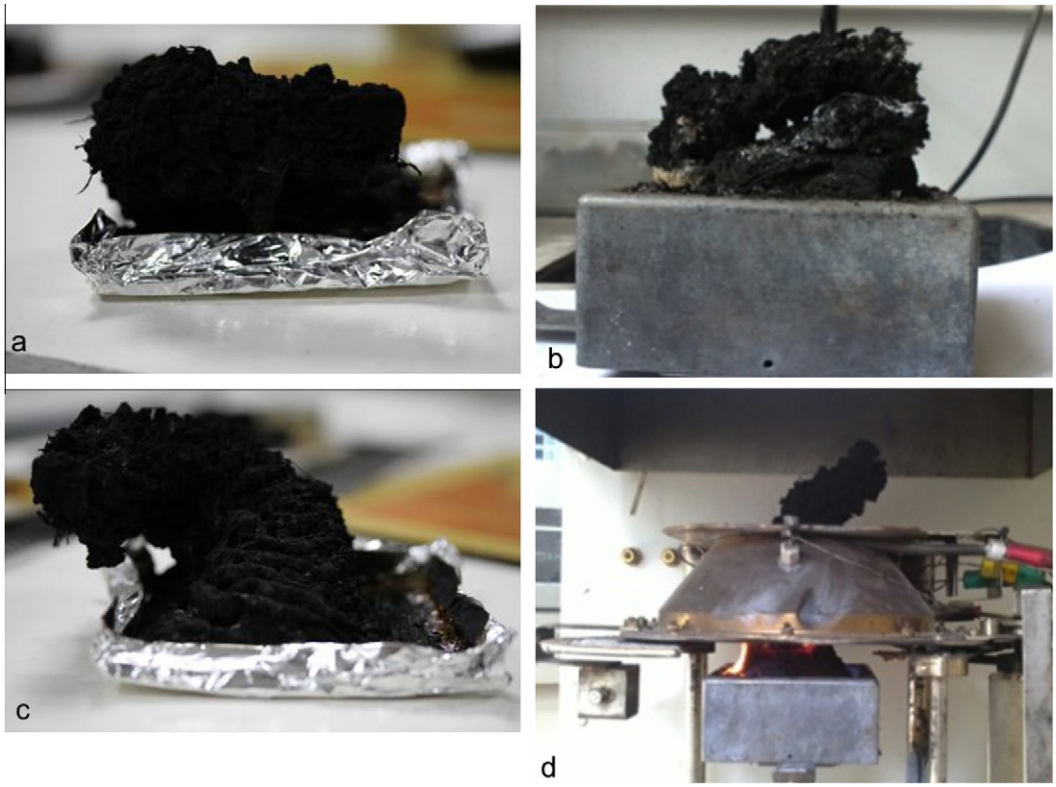

Fig. 7. Photographs of the residues remaining after the cone calorimeter test, (a) PC, (b) PC/POSS, (c) PC/RDP and (d) PC/POSS/RDP samples.

likely to occur in the combustion temperature range (around 700 °C at cone calorimeter test), and appears to act as a protective layer during the combustion.

3.2.5. Comparison between microcalorimeter and cone calorimeter data

It has been highlighted in the literature that PCFC is more adapted to study chemical decomposition processes than physical ones (mass or heat transfer barrier effects) taking place in the condensed phase [32–34]. Therefore,

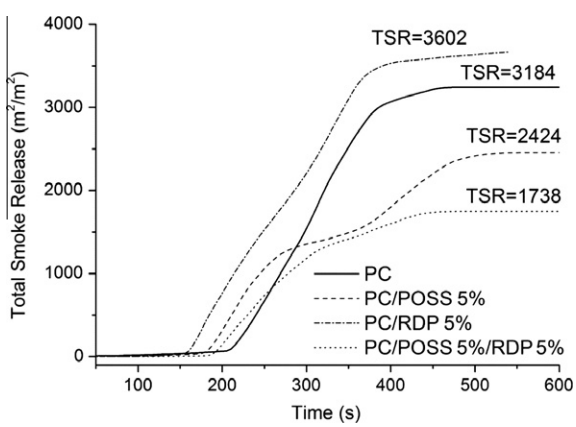

Fig. 8. Comparison of total smoke release (TSR) for PC, PC/POSS, PC/RDP and PC/POSS/RDP samples.

it has been shown, in a previous paper, that the comparison between microcalorimeter and cone calorimeter data can bring useful information about the physical action (especially the barrier effect) of flame retardant additives. It was assumed that the barrier effect is only active in cone calorimeter test and negligible in PCFC due to the small sample size [35]. Thus, it was supposed that the decrease of pHRR in cone calorimeter test (because of the incorporation of FR) should be higher (or at least equal to) than the decrease of pHRR (or Heat Release Capacity (HRC) (HRC is equal to the peak heat release rate (pHRR) divided by the heating rate)) in PCFC [35]. Here, the ratio between the HRC value of the flame retarded polymer sample in PCFC test (P–FR (PCFC)) and the HRC value of the non retarded polymer (P (PCFC)) is named R_1. (In this study, HRC is equal to pHRR due to presence of only one peak of HRR and a heating rate of 1 K s^{-1}).

$$R_1 = \frac{\text{HRC of P—FR(PCFC)}}{\text{HRC of P(PCFC)}}$$

The ratio between the pHRR of the flame-retarded polymer sample in cone calorimeter test (P–FR (cone calorimeter)) and the pHRR of the non-retarded polymer (P (cone calorimeter)) is named R_2.

$$R_2 = \frac{\text{pHRR of P—FR(cone calorimeter)}}{\text{pHRR of P(cone calorimeter)}}$$

Fig. 10 shows the representation of calculated R_2 values (X-axis) versus calculated R_1 values (Y-axis). For all FR

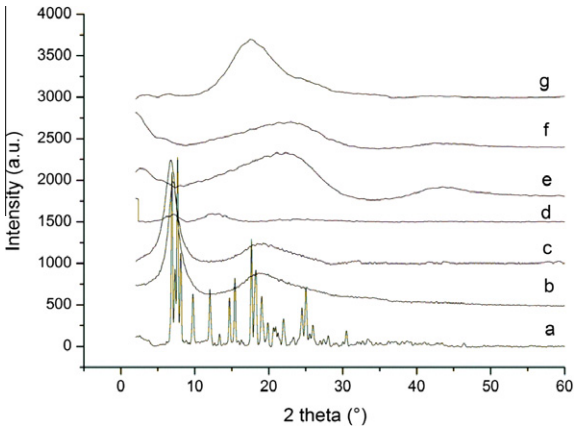

Fig. 9. XRD spectra of initial POSS (a) heated POSS 200 °C (b), 400 °C (c) and 700 °C (d), PC residue (e), PC–POSS-RDP residue top (f) PC–POSS–RDP residue botton (g).

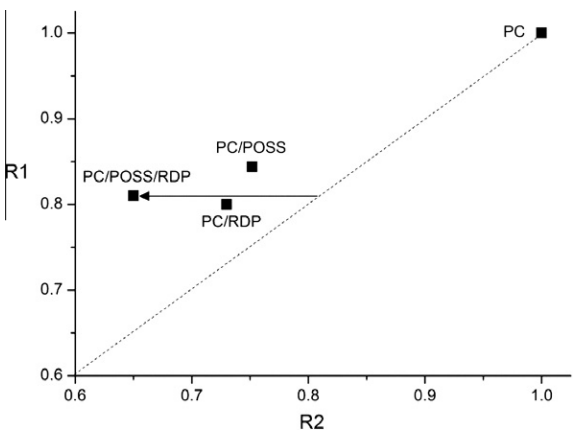

Fig. 10. R_1 versus R_2 representation for PC, PC/POSS, PC/RDP and PC/POSS/RDP samples.

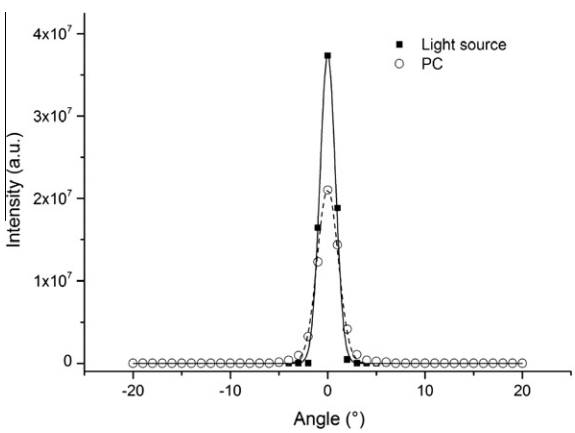

Fig. 11. Example of transmitted intensity peak profile fits (ordinates in arbitrary units, data as symbols and fitted Gaussians as lines): light source (circles and plain line) and PC sample (squares and dashed line).

Table 3
Physical transparency measurements: measured transmittance and angular dispersion, reconstructed ASTM and Haze Gard clarities.

Composition	T (%)	σ	ASTM D1746	Haze gard plus
No sample	–	0.7	100	100
PC	85	0.7	83.1	97.6
PC/RDP	64.3	0.7	60.3	90.3
PC/POSS	5.1	9.2	0.4	25
PC/POSS/RDP	3.5	10.3	0.25	24

Table 4
Measured psychophysical transparency parameters (distance between sample and background is 40 mm).

Composition	a	b	p	q	$\alpha\ (p-q)/(a-b)$	$t\ (aq-bp)/(a-b)$
No sample	246.4	40.6	246.4	40.6	1.00	0.00
PC	254.6	14.6	252.8	19.9	0.97	5.73
PC/POSS	254.4	16.8	198.4	69.7	0.54	60.60
PC/POSS/RDP	254.6	17.8	171.6	53.0	0.50	44.08

samples, the points are plotted above the dotted line $R_1 = R_2$ (This line corresponds to a similar decrease in pHRR in cone calorimetry and in PCFC).The great mismatch between experimental values and the dotted line $R_1 = R_2$ indicates that the barrier effect plays an important role in flame retardancy of these samples. The effect is particularly emphasized in the PC/POSS/RDP system. In this composition, it can be seen that, among the 35% decrease of pHRR in cone calorimeter, 15% may be attributed to the barrier effect (see the arrow on Fig. 10).

Finally, it can be concluded that combining POSS and RDP in PC leads to an improvement of the fire behavior through a synergistic action in the condensed phase. This synergy can be explained (i) by interactions between the additives and the polymer matrix during the decomposition leading to a reduction of the degradation rate, (ii) by a physical barrier effect that results from the formation of a cohesive char during combustion.

3.3. Transparency

3.3.1. Physical transparency

Although transparency relates to well known physical parameters (such as the absorption and scattering coefficients), quantification of physical transparency of materials is still controversial among researchers [36]. This is reflected in the various instruments and standards used for clarity measurements, with methods based on one intensity value (ASTM D 1746 [37]), two or more intensity values (Byk-Gardner Haze Gard Plus), integration of goniometric intensity data, or images of light distribution [38,39]. As demonstrated by Koo [36], results can be rather inconsistent and may lead to discordant decisions when comparing samples depending on the instrument used. In this work, both angular dispersion around the specular transmission direction and intensity were measured. As transmission peaks are found to be very close to Gaussians, angular dispersion may be expressed by a single standard deviation value (σ), while total intensities are given by

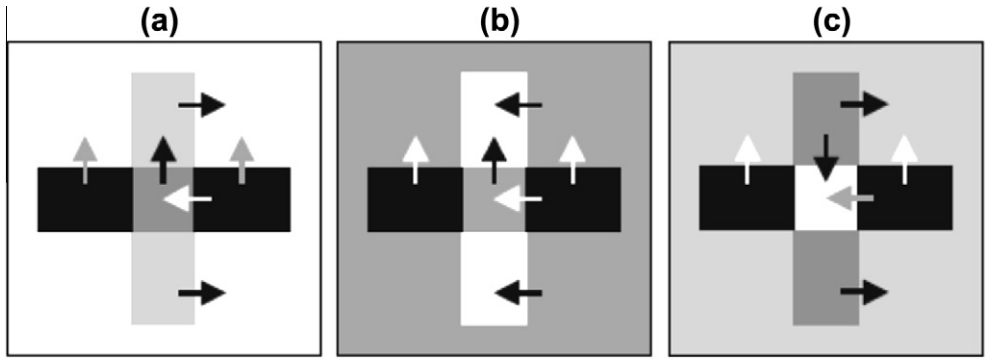

Fig. 12. X-junctions between superposed dark and light objects. Arrows indicate polarity (from dark to light). The number of polarity inversions result in judgements of unique transparency (a: grey is transparent), bistable transparency (b: any object may be transparent and lying above the other), and no transparency (c). Taken from [22], after Anderson [40].

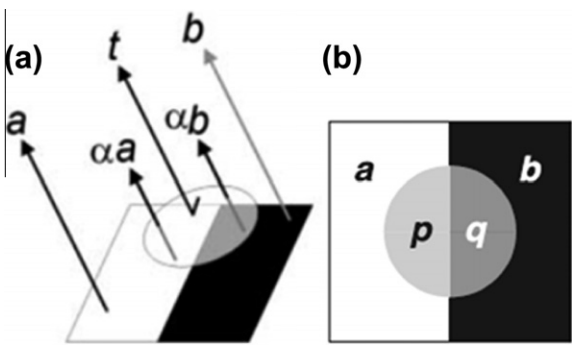

Fig. 13. definitions (a) and measurement zones (b) for α and t calculations in Table 4 (grey transparent object over a larger contrasting black-and-white background).

the peak areas (Fig. 11). Transmittance is expressed as the ratio of these intensities to the peak area obtained from the light source alone. ASTM and Haze Gard Plus clarities are reconstructed from angular measurements according to the instruments characteristics. Table 3 gives both measured and estimated values. Clarity evaluations are consistent with Koo's findings [36]. PC/POSS and PC/POSS/RDP samples have poor transmittance and strong dispersion. Examination between two crossed polarizing films shows textural features (flow lines, variations in particle orientation and matrix refractive index variations due to the injection process) that explain that most of the light flux is diffused outside the measurement spot of the instrument, but also that images observed through samples appear blurred and desaturated. The forming process (Injection molding), more than the material, is responsible for these low transparency characteristics.

3.3.2. Psychophysical transparency

Perception of transparency may involve many dimensions, such as specular reflection on the front surface of samples, background color and contrast (dynamics) alteration, and "milky" appearance due to light scattering inside the sample or to sample roughness. Psychophysically, the problem can be related to contrast perception. Current models connect works using X-junctions (perpendicular boundaries of transparent object and background contrasting features, Fig. 12) [40] to luminance-based models. Kitaoka [21] has used luminance measurement on four different areas (denoted a, b, p and q) of a scene including a transparent sample overlaying a black-and-white background (Fig. 13). Parameters α and t are said to account for, respectively, transmittance and glare (i.e. luminance depending on reflection from the transparent surface) of the sample. As a consequence, limit values of $\alpha = 1$ and $t = 0$ indicate absence of object, or an "invisible" object. Transparent objects with same α would be judged more transparent if having lower t values.

Table 4 shows that PC exhibits, as expected, a very good perceived transparency, together with a noticeable but still acceptable glare. PC/POSS and PC/POSS/RDP exhibit a lower transmittance than pure PC. However, by comparing Table 4 and Table 3, it can be noticed that the perceived transparency is much higher than the physical one. Although the PC/POSS samples appears as slightly more transparent than PC/POSS/RDP, it also looks "milkier", resulting in a translucent rather than transparent sample.

4. Conclusion

In this study, the combination of POSS and RDP into PC was performed in order to improve the flame retardancy of this matrix without affecting its transparency. It was shown that the presence of RDP appears to decrease slightly the aggregation of POSS particles and thus improve their dispersion in the matrix compared to PC/POSS blend. TGA results have highlighted that PC/POSS/RDP sample exhibits a reduced rate of degradation and an increased residue amount compared to PC, PC/POSS and PC/RDP. Both effects were related to the reactivity between the additives and the decomposing matrix. The synergistic action of POSS and RDP was assigned to the better dispersion of POSS in PC. The cone calorimeter test has shown that PC/POSS/RDP sample exhibits also the best flame retardancy performance with a low HRR and an important quantity of char residue. The comparison of cone calorimeter and PCFC results has revealed that the improved fire behavior

can be attributed to a barrier effect generated by the large char residue during combustion. Dealing with the optical properties, it seems that the injection molding process, more than the added materials (RDP, POSS), is responsible for decreasing of physical transparency characteristics. Evaluation of psychophysical transparency revealed the difference between perceived and physical transparency. Therefore, it is important to consider two approaches for characterization of transparency of composites. It was shown that PC/POSS/RDP composition can be considered as translucent rather than transparent due to light scattering.

Appendix A. Supplementary data

Supplementary data associated with this article can be found, in the online version, at http://dx.doi.org/10.1016/j.eurpolymj.2012.10.031.

References

[1] Bozi J, Czégény Z, Mészáros E, Blazsó M. Thermal decomposition of flame retarded polycarbonates. J Anal Appl Pyrolysis 2007;79:337–45.
[2] Zhang W, Li X, Guo X, Yang R. Mechanical and thermal properties and flame retardancy of phosphoruscontaining polyhedral oligomeric silsesquioxane (DOPO–POSS)/polycarbonate composites. Polym Degrad Stab 2010;95:2541–6.
[3] Levchik SV, Weil ED. Overview of recent developments in the flame retardancy of polycarbonates. Polym Int 2005;54:981–98.
[4] Steigerwald DA, Bhat JC, Collins D, Fletcher RM, Holcomb MO, Ludowise MJ, et al. Illumination with solid state lighting technology. IEEE J Sel Top Quantum 2002;8:310–20.
[5] Douce J, Boilot JP, Biteau J, Scodellaro L, Jimenez A. Effect of filler size and surface condition of nano-sized silica particles in polysiloxane coatings. Thin Solid Films 2004;466:114–22.
[6] Jang J, Oh JH. Fabrication of a highly transparent conductive thin film from polypyrrole/poly(methyl methacrylate), core/shell nanospheres. Adv Funct Mater 2005;15:494–502.
[7] Schulz H, Mädler L, Pratsinis SE, Burtscher P, Moszner N. Transparent nanocomposites of radiopaque, flame-madeTa$_2$O$_5$/SiO$_2$ particles in an acrylic matrix. Adv Funct Mater 2005;15:830–7.
[8] Deng Y, Gu A, Fang Z. The effect of morphology on the optical properties of transparent epoxy/montmorillonite composites. Polym Int 2004;53:85–91.
[9] Kiliaris P, Papaspyrides CD. Polymer/layered silicate (clay) nanocomposites: an overview of flame retardancy. Prog Polym Sci 2010;35:902–58.
[10] Feng J, Hao J, Du J, Yang R. Effects of organoclay modifiers on the flammability, thermal and mechanical properties of polycarbonate nanocomposites filled with a phosphate and organoclays. Polym Degrad Stab 2012;97:108–17.
[11] Feng J, Hao J, Du J, Yang R. Flame retardancy and thermal properties of solid bisphenol A bis(diphenyl phosphate) combined with montmorillonite in polycarbonate. Polym Degrad Stab 2010;95:2041–8.
[12] Imai Y, Terahara A, Hakuta Y, Matsui K, Hayashi H, Ueno N. Transparent poly(bisphenol A carbonate)-based nanocomposites with high refractive index nanoparticles. Eur Polym J 2009;45:630–8.
[13] Hakimelahi HR, Hu L, Rupp BB, Coleman MR. Synthesis and characterization of transparent alumina reinforced polycarbonate nanocomposite. Polymer 2010;51:2494–502.
[14] Krell A, Hutzler T, Klimke J. Transmission physics and consequences for materials selection, manufacturing, and applications. J Eur Ceram Soc 2008;29:207–21.
[15] Gnanasekaran D, Madhavan K, Reddy BSR. Developments of polyhedral oligomeric silsesquioxanes (POSS). POSS nanocomposites and their applications: A review. JSIR 2009;68:437–64.
[16] Zhao Y, Schiraldi DA. Thermal and mechanical properties of polyhedral oligomeric silsesquioxane (POSS)/polycarbonate composites. Polymer 2005;46:11640–7.
[17] Li L, Li X, Yang R. Mechanical, thermal properties and flame retardancy of PC/ultrafine octaphenyl-POSS composites. J Appl Polym Sci 2012;124(5):3807–14.
[18] Jiang Y, Li X, Yang R. Polycarbonate composites flame retarded by poly(phenylsilsesquioxane). In: Preceding of 22nd Annual Conference on Recent Advances on Flame Retardancy of Polymeric Materials. NY: USA; 2011.
[19] Yang F, Nelson GL. Combination effect of nanoparticles with flame retardants on the flammability of nanocomposites. Polym Degrad Stab 2011;96:270–6.
[20] Song L, Xuan S, Wang X, Hu Y. Flame retardancy and thermal degradation behaviors of phosphate in combination with POSS in polylactide composites. Thermochim Acta 2012;527:1–7.
[21] Liu YL, Chang GP, Hsu KY, Chang FC. Epoxy/polyhedral oligomeric silsesquioxane nanocomposites from octakis(glycidyldimethylsiloxy) octasilsesquioxane and small-molecule curing agents curing agents. J Polym Sci, Part A: Polym Chem 2006;44:3825–35.
[22] Kitaoka A. A new explanation of perceptual transparency connecting the X-junction contrast-polarity model with the luminance-based arithmetic model. JPN Psychol Res 2005;47:175–87.
[23] R Development Core Team, R: A language and environment for statistical computing, R Foundation for Statistical Computing. Vienna, Austria, ISBN 3-900051-07-0; 2011.
[24] Sánchez-Soto M, Schiraldi DA, Illescas S. Study of the morphology and properties of melt-mixed polycarbonate–POSS nanocomposites. Eur Polym J 2009;45:341–52.
[25] Wang J, Xin Z. Flame retardancy, thermal, rheological, and mechanical properties of polycarbonate/polysilsesquioxane system. J Appl Polym Sci 2010;115:330–7.
[26] Pack S, Kashiwagi T, Cao C, Korach CS, Lewin M, Rafailovich MH. Role of surface interactions in the synergizing polymer/clay flame retardant properties. Macromolecules 2010;43:5338–51.
[27] Modro AM, Modro TA. The phosphoryl and the carbonyl group as hydrogen bond acceptors. Can J Chem 1999;77:890–4.
[28] Murashko EA, Levchik GF, Levchik SV, Bright DA, Dashevsky S. Fire-retardant action of resorcinol bis(diphenyl phosphate) in pc–abs blend. II. Reactions in the condensed phase. J Appl Polym Sci 1999;71:1863–72.
[29] Song L, He Q, Hu Y, Chen H, Liu L. Study on thermal degradation and combustion behaviors of PC/POSS hybrids. Polym Degrad Stab 2008;93:627–39.
[30] Schartel B, Hull TR. Development of fire-retarded materials-interpretation of cone calorimeter data. Fire Mater 2007;31:327–54.
[31] Liang K, Li G, Toghiani H, Koo JH, Pittman CU. Cyanate ester/polyhedral oligomeric silsesquioxane (POSS)nanocomposites: synthesis and characterization. Chem Mater 2006;18:301–12.
[32] Schartel B, Pawlowski KH, Lyon RE. Pyrolysis combustion flow calorimeter: a tool to assess flame retarded PC/ABS materials? Thermochim Acta 2007;462:1–14.
[33] Morgan AB, Galaska M. Microcombustion calorimetry as a tool for screening flame retardancy in epoxy. Polym Adv Technol 2008;19:530–46.
[34] Tibiletti L, Longuet C, Ferry L, Coutelen P, Mas A, Robin JJ, et al. Thermal degradation and fire behaviour of unsaturated polyesters filled with metallic oxides. Polym Degrad Stab 2011;96:67–75.
[35] Sonnier R, Ferry L, Longuet C, Laoutid F, Friederich B, Laachachi A, et al. Combining cone calorimeter and PCFC to determine the mode of action of flame-retardant additives. Polym Adv Technol 2011;22:1091–9.
[36] Koo A. Clarity: current measurement practice. In: 2nd CIE Expert Symposium on Appearance, Ghent, Belgium, 8–10 September 2010.
[37] ASTM D1746-09 Standard test method for transparency of plastic sheeting, ASTM International, West Conshohocken, PA, DOI: 10.1520/D1746-09. <www.astm.org>.
[38] Wilchinsky ZW. Clarity measurement of polymer films. J Appl Polym Sci 1961;5:48–52.
[39] Ross G, Birley AW. Optical properties of polymeric materials and their measurement. J Phys D 1973;6:795.
[40] Anderson BL. A theory of illusory lightness and transparency in monocular and binocular images: the role of contour junctions. Perception 1997;26:419–53.